CWE-8
June 7-11, 2026
London, ON, Canada

CFD and PIV comparison of the anisotropy of turbulence in the wake of a cyclist

Jose Arbelo Romero [a*], Sajad Maleki Dastjerdi[b], Bert Blocken[c], Hassan Hemida[a], Mark Sterling[d], Wouter Terra[b], Andrea Sciacchitano[b], Thijs van Druenen[e]

[a]*University of Birmingham, Birmingham, United Kingdom*
[b]*Delft University of Technology, Delft, the Netherlands*
[c]*Heriot-Watt University, Edinburgh, United Kingdom*
[d]*Manchester Metropolitan University, Manchester, United Kingdom*
[e]*Eindhoven University of Technology, Eindhoven, the Netherlands*
**Corresponding author: JMA337@student.bham.ac.uk*

SUMMARY

For the first time, the anisotropy of turbulence in the wake of a cyclist in time trial position is presented by means of contours of states of anisotropy and barycentric anisotropic invariant maps. Results obtained from Particle Image Velocimetry (PIV) and steady RANS CFD simulations are compared, highlighting some of the deficiencies in linear eddy-viscosity models used for turbulence modelling. The motivation is twofold: Anisotropy of turbulence influences turbulence momentum transport, therefore an improved understanding of the characteristics of turbulence in the wake may inform strategies in cycling or fabric development. In addition, information about the dominant turbulence components is useful in developing and tuning of turbulence closure models.

Keywords: *Computational fluid dynamics (CFD), Particle Image Velocimetry (PIV), sports aerodynamics*

1. INTRODUCTION

The anisotropy of turbulence is the mechanism by which turbulence transports momentum and other scalar fluxes (Pope, 2000). Analysing the anisotropy of turbulence offers a complementary view of turbulence, revealing information not obviously observed in the physical space, and can help identify the sources and mechanisms of turbulence production. The specific Reynolds stress tensor, $\tau_{ij} = \overline{u_i{}' u_j{}'}$, can be decomposed into an isotropic and anisotropic (traceless deviatoric) contribution, such that the anisotropic Reynolds stress tensor is defined as $a_{ij} = \overline{u_i{}' u_j{}'} - \frac{2}{3} k \delta_{ij}$. Where the overbar terms denotes time/ensemble average, $u_i{}'$ and $u_j{}'$ are the fluctuating velocity components, the indices i and j in Einstein notation are free indices that take on values 1, 2, and 3 (representing the x, y, z spatial dimensions), k is the turbulent kinetic energy and δ_{ij} is the Kronecker delta. The normalized anisotropic Reynolds stress tensor is defined as $b_{ij} = \frac{a_{ij}}{2k} = \frac{\overline{u_i{}' u_j{}'}}{2k} - \frac{1}{3}\delta_{ij}$. In CFD simulations using the incompressible 3D Reynolds-Averaged Navier Stokes equations (RANS), the unresolved part of the Reynolds stress tensor can be modelled in terms of mean-velocity gradients ($\frac{\partial U_i}{\partial x_j}$) using the linear eddy-viscosity (ν_t) Boussinesq assumption.

Employing invariant analysis and eigendecomposition of b_{ij}, an anisotropy invariant map (AIM) can be constructed to characterise the states of turbulence. AIMs give no information about the physical shape of the eddies, but about the relative strength between components of the Reynolds stress tensor. Using the method proposed by Banerjee et al. (2007) and Emory and Iaccarino (2014), barycentric AIMs and contours of the state of anisotropy respectively, the anisotropy of

turbulence is observable in physical space, and so is the non-uniformity of the momentum transport by the turbulent fluctuations. The current research work provides insights into the convection of turbulence anisotropy in the wake of a cyclist by means of Particle Image Velocimetry (PIV) and compares these to a steady RANS CFD simulation. Results are compared based on contours of states of anisotropy in two planes in the wake of the cyclist, and the corresponding barycentric AIMs. Results for unsteady RANS and scale resolving CFD simulations are expected to be available by the time of the conference.

2. METHODOLOGY

2.1. Wind tunnel measurements

Wind tunnel (WT) measurements were conducted in the open jet facility (OJF), a closed-circuit and open test-section wind-tunnel facility at TU Delft, the Netherlands. The test-section has an octagonal nozzle of 2.85 x 2.85 m^2. Figure 1 provides a schematic representation of the experimental campaign setup and the location of such measurement volumes. The generic cyclist model (GCM) introduced by Terra et al. (2024), a full-scale cyclist mannequin in time trial position, was installed on a Scott Plasma 5 frame with rim brakes, a Shimano DuraAce wheelset and a Kask Mistral helmet (Figure 1). The GCM-bicycle system was mounted onto a six-component balance designed, manufactured and calibrated by the Dutch Aerospace Laboratory (NLR), via four frames connected to either side of the wheel-axles. The height (H) and length (L) of the mannequin-bicycle system was 1.37 m and 1.67 m, respectively. The freestream reference velocity (U_∞) was 14.0 m/s headwind (0° yaw). The boundary layer height was less than 5 cm, which was well below the feet of the cyclist. The freestream turbulence intensity (TI) at the WT test section was about 0.6%. The combined frontal area of the mannequin and bicycle was 0.35 m^2 at 0° yaw, yielding a blockage ratio of about 4%. The large-scale 3D PIV system consisted of sub-millimeter neutrally buoyant helium-filled soap bubbles (HFSB) flow tracers illuminated by four LaVision LED-Flashlight 300 and imaged by four Photron Fastcam Mini AX100 cameras (resolution of 1 megapixel) and 50 mm focal length Samyang lenses. A total of 10,000 images were acquired at a frequency of 1.0 kHz. The velocity field was retrieved via Lagrangian Particle Tracking (LPT) using the Shake-the-Box algorithm in the LaVision DaVis 10 software. Data were averaged in space and time over cubic volumes of size 48 voxels and an overlap of 75%. Two measurement volumes were considered: One just downstream the saddle, and another just downstream the rear wheel.

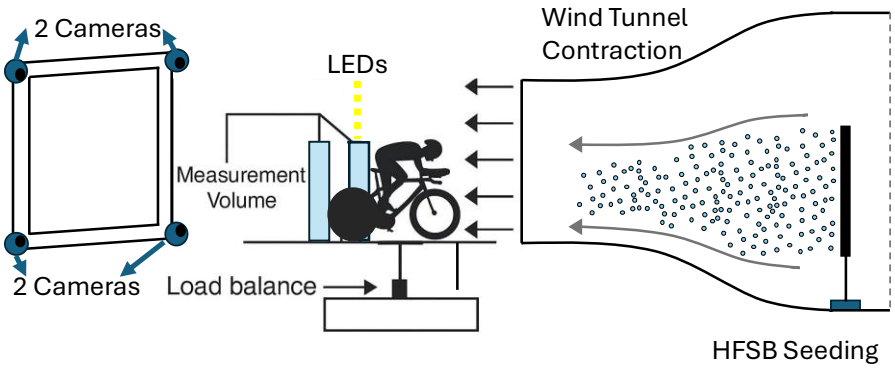

Figure 1: Schematic diagram of the experimental setup in the OJF, with the relevant components labelled.

2.2. CFD simulation set-up

The computational geometry of the cyclist and bicycle in this study was identical to that in the WT measurements. The computational domain is similar to the OJF, though the fetch downstream of the cyclist was extended to comply with CFD best practice guidelines. The domain, shown in Figure 2d, was discretised following a poly-hexcore grid topology, which connects prism cells in the boundary layer to octree hexahedral cells in the volume grid by polyhedral cells. The condition $y_p = 10$ μm was enforced to ensure that the average wall distance $\overline{y^+} \leq 1$. Due to flow acceleration, y^+ can locally reach values as large as 3. On the ground wall surface, 12 prismatic layers were used, with $\overline{y^+} \leq 5$. The total cell count was 98×10^6. The 3D steady RANS equations were closed with the 4-equation transition SST (TSST) model. Curvature corrections and production limiters with clip factor 10 were included. The Coupled algorithm was used as a full implicit pressure-velocity coupling, together with pseudo-transient underrelaxation. The pseudo time step was set to 0.01 s. Gradient interpolation was taken care of by the Green-Gauss node-based method, and second order schemes were used for spatial discretisation. The simulation was first initialised for 2,000 pseudo time steps, after which data sampling was started and the simulations were terminated once the moving average of the C_DA had converged (deviations < 0.05%), which required 8,000 pseudo time-steps.

3. RESULTS

All realizable anisotropy invariant combinations must lie in the area defined in the barycentric AIM triangular map between the three boundaries, which mark the limiting physical bounding states of turbulence. Each corner represents a limiting state: one-component (1C), two-component axisymmetric (2C) and three-component isotropic (3C). The boundaries connecting the limiting states describe further states. Figure 3 displays contours of the anisotropy of turbulence and corresponding barycentric AIMs in plane 1 and plane 2, which correspond to just downstream of the saddle and the rear wheel, respectively. In general, significantly more anisotropy of turbulence is captured by PIV (Figure 3a) than by RANS (Figure 3b). As seen in plane 1 for Figure 3a, the near wake is dominated by 1C turbulence state (one direction of the Reynolds stress tensor dominates over the other two) and axisymmetric expansion, which is characteristic of the edges of mixing/shear layers (Minguez and Pasquetti, 2008). There are also some noticeable regions of 2C state visible towards the centerline of the cyclist in the lower back region, possibly due to the strain caused by the strong downwash acceleration (Minguez and Pasquetti, 2008). Additionally, a general return to isotropy is seen in plane 2 as the wake convects downstream from plane 1. Figure 3b shows RANS mainly predicts isotropic turbulence, though some 3C and axisymmetric contraction states are predicted around the straight leg, in contrast to the PIV results, possibly because of the isotropic scalar eddy-viscosity assumption in the Boussinesq assumption.

4. CONCLUSIONS

For the first time, the anisotropy of turbulence in the wake of a cyclist in time trial. By means of contours of states of anisotropy and barycentric anisotropic invariant maps, results obtained from Particle Image Velocimetry (PIV) are compare steady RANS CFD simulations, highlighting some of the deficiencies in linear eddy-viscosity models used for turbulence modelling.

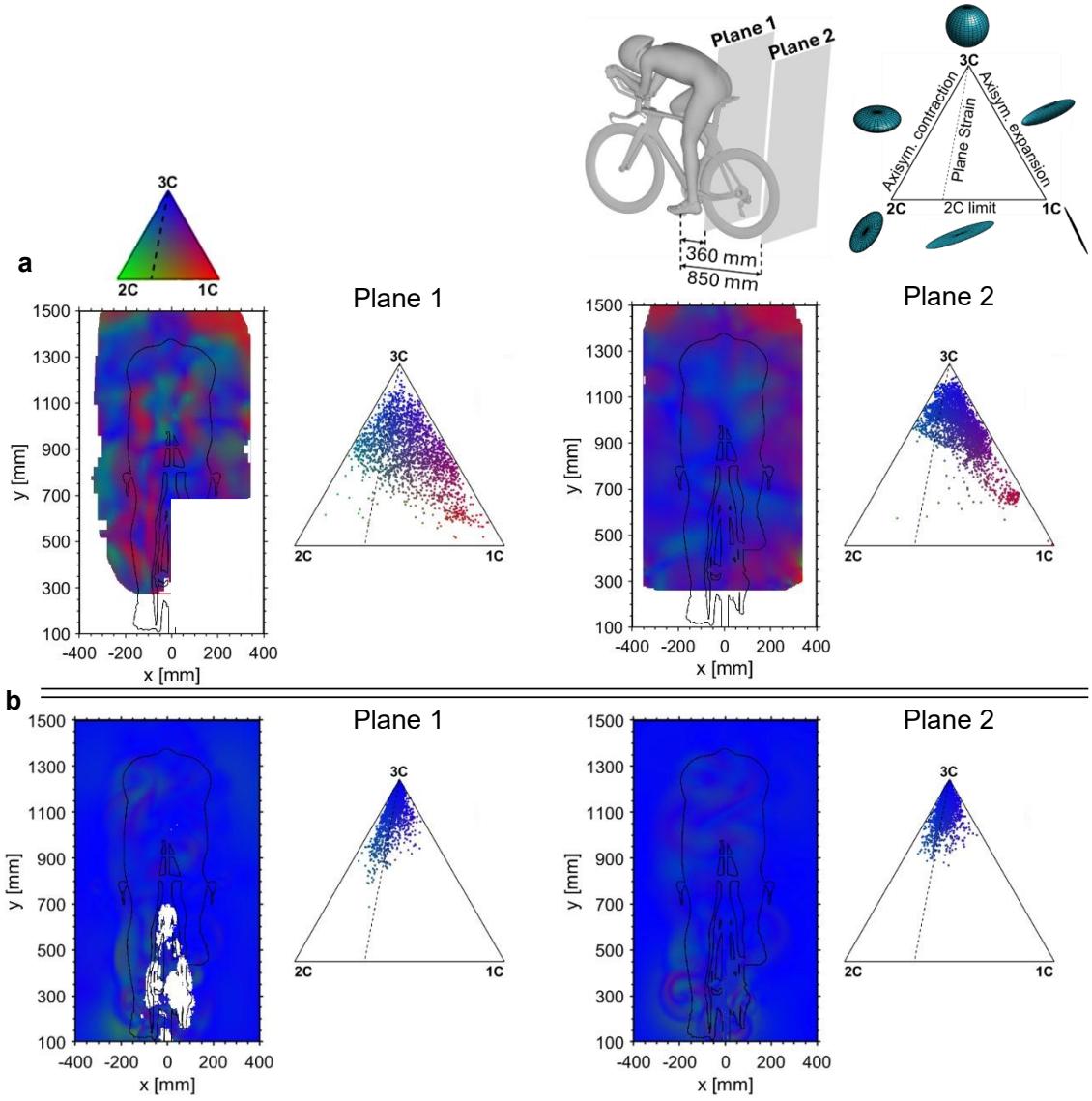

Figure 3: Contours of the anisotropy of turbulence and barycentric AIMs in two x-y planes in the wake of the cyclist for: (a) PIV; (b) steady RANS CFD.

ACKNOWLEDGEMENTS

All simulations performed on the Birmingham Environment for Academic Research (BEAR) computational facility.

REFERENCES

Pope, S.B., 2001. Turbulent flows. *Measurement Science and Technology*, *12*(11).

Emory, M. and Iaccarino, G., 2014. Visualizing turbulence anisotropy in the spatial domain with componentality contours. *Center for Turbulence Research Annual Research Briefs*, pp.123-138.

Banerjee, S., Krahl, R., Durst, F. and Zenger, C., 2007. Presentation of anisotropy properties of turbulence, invariants versus eigenvalue approaches. *Journal of Turbulence*, (8), p.N32.

Terra, W., Brown, C., Vloemans, S., van der Waals, M., Sciacchitano, A., Burton, D., Thompson, M.C. and Huysmans, T., 2024. A Generic Cyclist Model for aerodynamic investigation: Design, geometry & first aerodynamic analysis of a male time-trial and sprint model. *Journal of Wind Engineering and Industrial Aerodynamics*, *252*.

Minguez, M., Pasquetti, R. and Serre, E., 2008. High-order large-eddy simulation of flow over the “Ahmed body” car model. *Physics of fluids*, *20*(9).